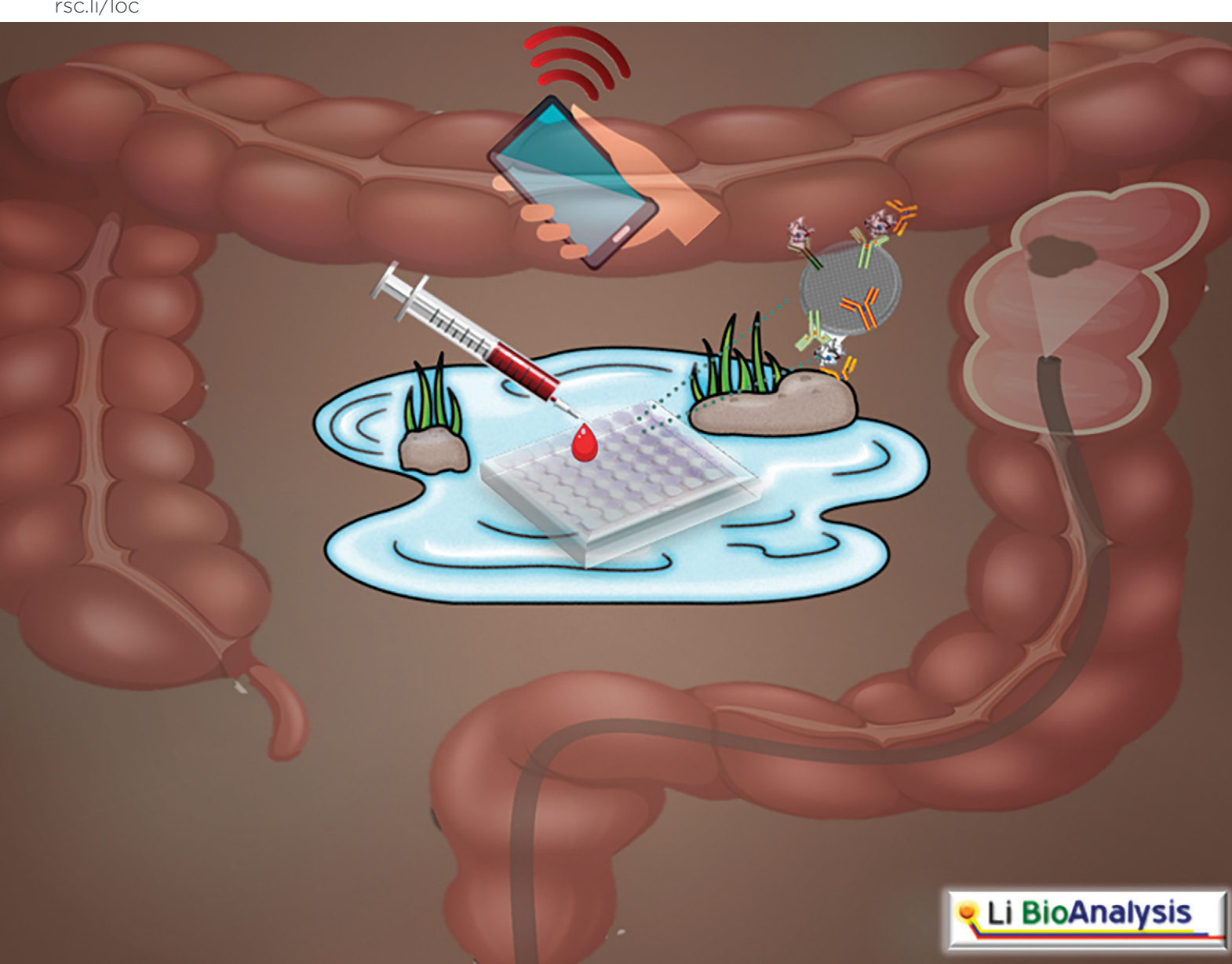
Volume 24 Number 21 7 November 2024 Pages 4933-5078

# Lab on a Chip

Devices and applications at the micro- and nanoscale rsc.li/loc



ISSN 1473-0197



#### **PAPER**

XiuJun Li *et al*.

A paper-in-polymer-pond (PiPP) hybrid microfluidic microplate for multiplexed ultrasensitive detection of cancer biomarkers

## Lab on a Chip



**PAPER** 

View Article Online



Cite this: Lab Chip, 2024, 24, 4962

## A paper-in-polymer-pond (PiPP) hybrid microfluidic microplate for multiplexed ultrasensitive detection of cancer biomarkers†

Sanjay S. Timilsina<sup>a</sup> and XiuJun Li \*\*D\*\*ab

Conventional affinity-based colorimetric enzyme-linked immunosorbent assay (ELISA) is one of the most widely used methods for the detection of biomarkers. However, rapid point-of-care (POC) detection of multiple cancer biomarkers by conventional ELISA is limited by long incubation time, large reagent volume, and costly instrumentation along with low sensitivity due to the nature of colorimetric methods. Herein, we have developed a reusable and cost-effective paper-in-polymer-pond (PiPP) hybrid microfluidic microplate for ultrasensitive and high-throughput multiplexed detection of disease biomarkers within an hour without using specialized instruments. A piece of pre-patterned chromatography paper placed in the PMMA polymer pond facilitates rapid protein immobilization to avoid intricate surface modifications of polymer and can be changed with a fresh paper layer to reuse the device. Reagents can be simply delivered from the top PMMA layer to multiple microwells in the middle PMMA layer via flow-through microwells, thereby increasing the efficiency of washing and avoiding repeated manual pipetting or costly robots. Quantitative colorimetric analysis was achieved by calculating the brightness of images scanned by an office scanner or a smartphone camera. Sandwich-type immunoassay was performed in the PiPP hybrid device after the optimization of multiple assay conditions. Limits of detection of 0.32 ng mL<sup>-1</sup> for carcinoembryonic antigen (CEA) and 0.20 ng mL<sup>-1</sup> for prostate-specific antigen (PSA) were obtained, which were about 10-fold better than those of commercial ELISA kits. We envisage that this simple but versatile hybrid device can have broad applications in various bioassays in resource-limited settings.

Received 2nd June 2024 Accepted 5th September 2024

DOI: 10.1039/d4lc00485j

rsc li/loc

#### **Tribute to George Whitesides**

I had the privilege of working as a postdoctoral fellow in Prof. George Whitesides' lab at Harvard University from January 2010 to December 2011, where I focused primarily on low-cost diagnostic technologies. This period of training was not only unforgettable but also profoundly shaped the direction of my subsequent independent research. For instance, low-cost diagnostics and point-of-care bioanalysis have become central themes in my research group at the University of Texas at El Paso since I joined in January 2012. In 2014, I was honored with the "Bioanalysis New Investigator Award", which was a testament to the strong foundation I gained during my time in Prof. Whitesides' lab. The diversity of research projects in his group offered me a great opportunity to explore multiple fields, including 3D cell culture. This experience laid the groundwork for my current exploration of a wide range of research areas—from biomedical to environmental applications—using microfluidics and nanotechnology. Thank you, George, for your mentorship and inspiration. Wishing you a very happy 85th birthday!

Dr. Xiujun (James) Li

## 1. Introduction

Cancer figures among the leading causes of death worldwide, accounting for an estimated 19.31 million new cases and 10 million cancer deaths in 2020.1,2 Cancer is the second leading cause of death in the US, exceeded only by heart disease, accounting for nearly 1 of every 4 deaths.3 For instance, prostate cancer is the second most common cancer in men in the US.4 Worldwide, in 2020 an estimated 1.42 million people were diagnosed with prostate cancer with 375 304 associated deaths which account for roughly 7.3% of cancer incidence. 1,2,5 Likewise, colorectal cancer is the third most common cancer with around 1.9 million cases, which is around 10% of total cancer cases.5 Total mortality is estimated to be 935 000 per year in both sexes in 2020.<sup>2,5,6</sup> Although most countries with top incidence rates for cancer

<sup>&</sup>lt;sup>a</sup> Department of Chemistry & Biochemistry, University of Texas at El Paso, 500 W University Ave, El Paso, TX, USA. E-mail: xli4@utep.edu

<sup>&</sup>lt;sup>b</sup> Forensic Science & Environmental Science and Engineering, 500 W University Ave, El Paso TX USA

<sup>†</sup> Electronic supplementary information (ESI) available. See DOI: https://doi.org/ 10.1039/d4lc00485j

Lab on a Chip

are developed countries, the highest mortality rate occurs in developing countries. The higher mortality in developing countries is mainly due to late diagnosis and access barriers to diagnosis and medical care.7 For instance, the incidence of prostate and colorectal cancer remains highest in developed countries like Australia and North America and remains low in the Asian population, eastern and South Central Asia, and Western Africa. However, mortality is higher in less developed regions due to poor prognosis.<sup>2</sup> The global cancer burden is expected to be 28.4 million cases in 2040, a 47% rise from 2020, with a larger increase in transitioning (64% to 95%) versus transitioned (32% to 56%) countries due to demographic changes. Also, the share of cancer deaths in Asia (58.3%) and Africa (7.2%) was found to be higher than the share of incidence (49.3% and 5.7%).8 In addition, cancer also causes a tremendous burden on society in terms of economic cost.<sup>9,10</sup> According to a recent study, the global burden of colorectal cancer is expected to increase by 60% to more than 2.2 million new cases and 1.1 million deaths by 2030.11 Therefore, there is an urgent need for low-

cost diagnostic methods for cancer early detection.

Early detection of cancer biomarker proteins holds immense potential to increasing cancer survival rates and monitoring of cancer treatment or personalized therapy. 12 To achieve high specificity of cancer early diagnosis, multiplexed biomarker detection is usually needed. Additionally, multiple types of cancer can coexist. For example, some studies show that men with prostate cancer have a higher risk of developing colon cancer and vice versa. 13 However, conventional cancer biomarker detection methods including enzyme-linked immunosorbent assay (ELISA) and western blotting are limited for multiplexed quantitative cancer biomarker detection in low-resource settings such as developing nations and small clinics,14-16 either by long analysis time, large sample volume required, costly instruments, need for well-trained personnel, or complexity for routine diagnosis. Furthermore, very low concentrations of cancer biomarkers are frequently encountered in earlystage tumors. Hence, it is important to develop low-cost and sensitive multiplexed quantitative biomarker detection methods suitable for low-resource settings for early cancer diagnosis.

The microfluidic lab-on-a-chip (LOC) technique that consumes minimum volume of samples and integrates multiple functional units possesses remarkable features such as low cost, rapid processing and detection, high portability, high sensitivity and throughput analysis of complex biological fluids<sup>15,17-22</sup> providing a versatile platform for POC detection.23,24 The World Health Organization's guidelines have defined criteria of POC devices as ASSURED (affordable, sensitive, specific, user-friendly, rapid treatment and robust use, equipment free and delivered to those in need).<sup>25</sup> Several microfluidic devices have been reported for the immunoassay of PSA (a prostate cancer biomarker)26 and CEA (a colon cancer biomarker)27 using different detection techniques such as colorimetric, luminescence,

electrochemical, and fluorescence detection. 28-34 For instance, Zhou et al. performed a paper-based colorimetric assay for the detection of PSA. The process required complicated and time-consuming cross-linking of siloxane 3-aminopropyltriethoxysilane and glutaraldehyde to the filter paper followed by a coating of the chitosan layer and adsorption of gold nanoparticles. The assay also required several hours to be completed.<sup>28</sup> Barbosa et al. used carbon and gold nanoparticles as immunoassay labels for PSA detection with optical detection in a FEP Teflon polymer microfluidic POC platform called microcapillary film but the dynamic range was limited to 10-100 ng mL<sup>-1</sup> higher than the clinical cutoff value, with an assay time of longer than 5 h.<sup>30</sup> Qiu et al. developed a quantum dot-enzyme-impregnated paper-based analytical device for visual fluorescence detection of CEA using mesoporous silica nanocontainers. The process involved complicated and time-consuming conjugation and surface modification of the paper substrate. Although the result could be viewed by the naked eye for qualitative analysis, a commercial fluorospectrometer was required for quantitative analysis.<sup>33</sup> Chen et al. performed multiplexed detection of PSA and CEA using a PDMS/glass microfluidic platform that integrated single bead trapping and acoustic mixing technique. It required a piezo transducer to generate fast-switching flow patterns, a syringe pump, a CCD camera and a mercury lamp, with a LOD of 3.1 ng mL<sup>-1</sup> for CEA.<sup>31</sup> Even though many of these methods are very selective and sensitive, they require extensive time to carry out the bioassay, complicated sample pretreatment, sophisticated surface modification and conjugation steps, and the use of bulky and costly instruments for detection. Other kinds of POC devices including agglutination and lateral flow assays usually lack the capability for quantitative result and multiplex detection. <sup>25,35</sup>

Herein, we have developed a paper-in-polymer-pond (PiPP) hybrid microfluidic device for low-cost detection of multiple cancer biomarkers with high detection sensitivity. Whatman grade 1 Chr chromatography paper which is uniform in structure and free of hydrophobic binders/coatings is an inexpensive and widely used microfluidic substrate.25,36 It provides fast biomolecule immobilization, but it does not offer high performance in flow control.25,37 Although acrylics and plastics are other widely used substrates, 38 they require surface modification for immobilization of the biomolecules. 39,40 Thus, the Li group introduced paper/polymer hybrid microfluidic devices that can draw more benefits from different substrates for different biomedical applications. 20,25,41,42 Herein, porous 3D paper with a high surface-to-volume ratio kept in a PMMA pond can easily immobilize/capture antibodies within 10 min, thereby decreasing the assay time to 1 h compared to nearly 16 h in traditional microplates. The presence of the pond-shaped structure avoids the addition of paper disks to individual microwells separately, as a single paper substrate cut by laser cutter in the shape of a pond can be added to the PiPP device. The flow-through pond also acts as an outlet channel to direct the waste reagents to outlet microwells. The vertical flowthrough reservoirs which pass through the paper substrate to

the outlet layer ensure maximum immobilization of the protein and efficient washing, thereby increasing the sensitivity and decreasing the background noise. Simultaneous sandwich-type multiplexed immunoassay of cancer biomarkers including PSA and CEA was performed in this hybrid device and 10-fold higher sensitivity than that of traditional microplates was obtained without the use of any sophisticated instruments like a

## 2. Experimental

microplate reader.

**Paper** 

#### 2.1 Chemicals and materials

ELISA: anti-rabbit IgG-alkaline phosphatase, Tween 20, albumin from bovine serum, polyclonal anti-carcinoembryonic antigen, monoclonal anti-carcinoembryonic antigen, prostate-specific antigen, serum from normal human male AB plasma, 5-bromo-4-chloro-3-indolyl phosphate + nitroblue tetrazolium (BCIP/NBT) liquid substrate, and phosphate-buffered saline (PBS) were

purchased from Sigma Aldrich (St. Louis, MO). Carcinoembryonic antigen, polyclonal anti-PSA, and monoclonal anti-PSA were purchased from Abcam (Cambridge, MA). Unless otherwise noted, all solutions were prepared with ultrapure Milli-Q water (18.2 M $\Omega$  cm) from a Millipore Milli-Q system (Bedford, MA).

Microfluidic platform fabrication: PMMA was purchased from McMaster-Carr (Los Angeles, CA). Whatman #1 chromatography paper was purchased from Sigma Aldrich (St. Louis, MO).

#### 2.2 Microfluidic platform design and fabrication

The microfluidic device used in this study was designed in Adobe Illustrator CS5 and fabricated using a 30 W CO<sub>2</sub> laser cutter (Epilog Zing 16, Golden, CO) with different speeds and power of the laser to create specific heights in raster mode as described in detail in our previous paper.<sup>25</sup> As seen in Fig. 1,

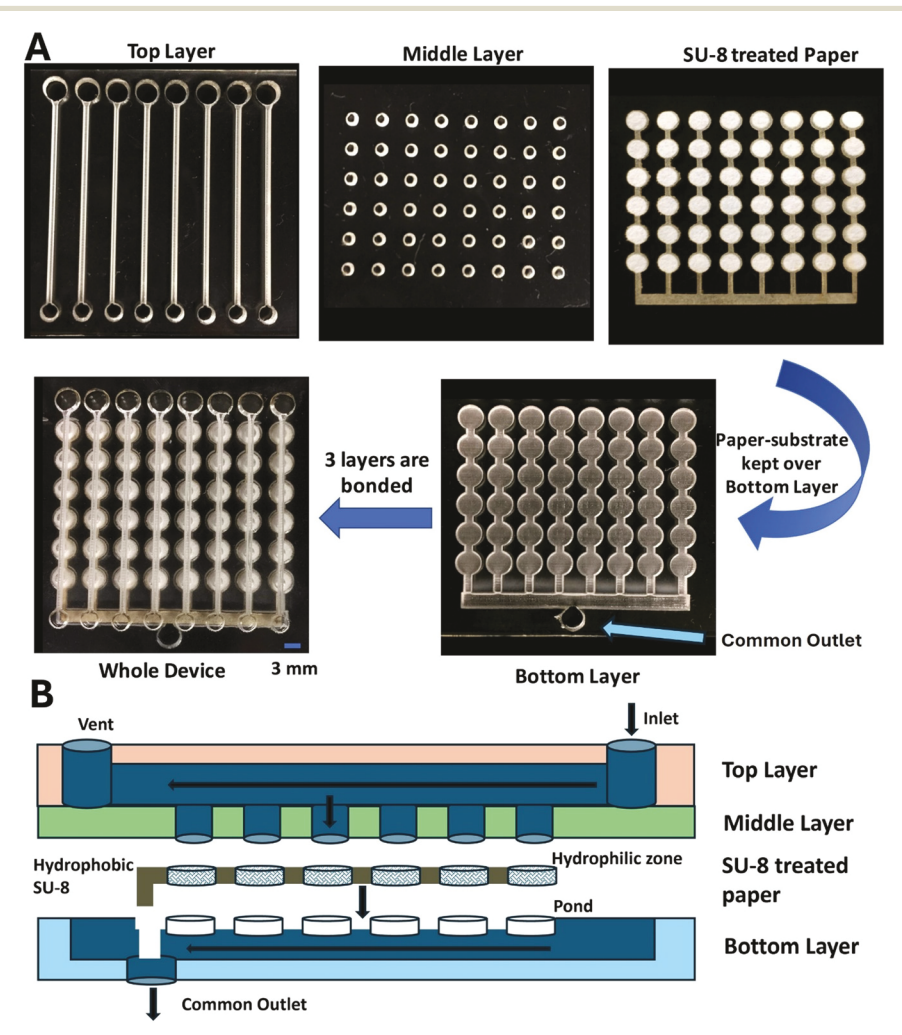


Fig. 1 Paper-in-polymer-pond (PiPP) hybrid microfluidic microplate. (A) Layout and fabrication procedures of the PiPP hybrid device in photographs. The PiPP hybrid device consists of a top PMMA layer, a middle PMMA layer, and a pond-structured bottom PMMA layer, and an SU-8 treated paper layer was kept over the bottom pond layer. The white areas in the paper are hydrophilic while the rest are hydrophobic due to the SU-8 treatment. The top PMMA layer has inlet microwells and reagent delivery channels which are kept in an inverted position. The middle layer has  $6 \times 8$  reservoirs. The bottom layer has a pond-shaped structure connected to a common outlet channel leading to an outlet microwell. (B) Schematic of the cross section of the PiPP hybrid microplate along one channel in an exploded view. The arrows indicate the flow path.

Lab on a Chip Paper

the device consists of three different PMMA layers. The top PMMA layer has eight different fluid delivery channels connected to each inlet microwell. The reagents added from the top reagent delivery layer flow through the fluid delivery channel into six reservoirs (2.0 mm diameter) kept just below each channel in the middle PMMA layer. The bottom PMMA layer of the device consists of interconnected pond-shaped structures. The pond-shaped structures (0.6 mm in height) in the same column are connected to each other. Finally, all the outlets for the ponds are connected to a common horizontal outlet which has a higher depth (1.5 mm) than the vertical outlet channels so that the waste reagent does not flow back to the same or different outlet channels. To generate the hydrophobic/hydrophilic zones on the paper layer, a piece of chromatography paper was treated with SU-82010 photoresist using the photolithography technique. 43 Briefly, a photomask was designed and printed on a transparency slide with a standard laser printer and aligned with the hydrophilic SU-8treated chromatography paper and exposed to UV radiation

(intensity 100%, 20 seconds). The SU-8-treated paper is cut by a laser cutter in the same pattern as the shape of the ponds and imbedded in the ponds of the bottom layer so that all the reservoirs in the middle PMMA layer fall just above the hydrophilic layer of the paper (3.5 mm in diameter). In this way, the reagent added from each inlet microwell flows through the channel to the six reservoirs below each channel and pass through the paper into the pond and to the outlet. All the reagents flow through the hydrophilic paper layer so that the maximum amount of protein is immobilized onto the surface of the paper substrate. The schematic in Fig. 1B shows the cross section of the PiPP device along one channel in an exploded view and the reagent flow path.

#### 2.3 Optimization of the concentration of capture antibody

The procedures of the colorimetric ELISA of PSA and CEA in this PiPP hybrid device are similar and were performed at room temperature. Thus, we use CEA as an example to

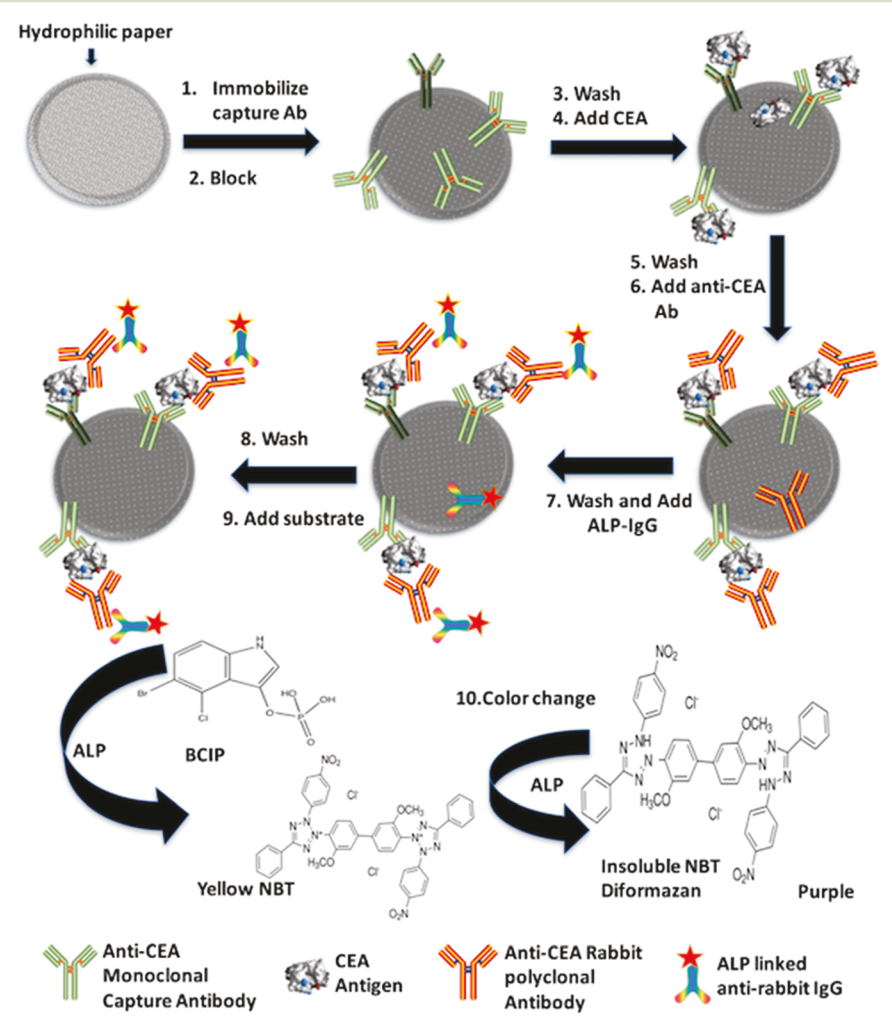


Fig. 2 Schematic of the colorimetric immunoassay principle for the visual quantitative detection of CEA on the PiPP hybrid device: (1) immobilizing of the monoclonal capture antibody in the paper substrate, (2) blocking, (3) washing, (4) addition of CEA, (5) washing, (6) addition of polyclonal anti-CEA antibody, (7) washing and addition of ALP-linked IgG, (8) washing, (9) addition of the substrate, and (10) enzymatic production of insoluble NBT diformazan.

**Paper** 

explain the procedures of the assay and its optimization, as illustrated in Fig. 2. For instance, the immunoassay of CEA was performed with different concentrations of anti-CEA capture antibody for the optimization of the concentration of capture antibody. First, different concentrations monoclonal anti-CEA capture antibody (1 μg mL<sup>-1</sup>, 5 μg  $mL^{-1}$ , 10  $\mu g$   $mL^{-1}$ , 15  $\mu g$   $mL^{-1}$ , 20  $\mu g$   $mL^{-1}$ , 25  $\mu g$ mL<sup>-1</sup>, and 30 μg mL<sup>-1</sup> in 10 mM PBS, pH 8.0) were added to the hybrid device and incubated for 10 min. The device was then blocked with a blocking buffer for another 10 min followed by washing with PBST (PBS with 0.05% Tween 20). Afterward, 500 ng mL<sup>-1</sup> CEA was added for the positive controls, while PBS was used for the negative control. After incubating the positive and negative control for 10 min, the device was washed with PBST before 10 µg mL<sup>-1</sup> polyclonal anti-CEA antibody was added. The device was washed with PBST after 10 min incubation followed by the addition of 10 μg mL<sup>-1</sup> ALP-linked IgG for 7 min. Finally, the device was washed three times with PBST and the colorimetric BCIP/NBT was added. The device disassembled 10 min after the addition of the substrate and the bottom pond layer with the paper substrate was scanned using an office scanner or a smartphone camera. ImageJ was used to obtain the brightness value which was used for further quantitative analysis.

# 2.4 Optimization of the concentration of anti-CEA polyclonal antibody

Optimization of the concentration of the anti-CEA polyclonal antibody was performed with the optimized concentration of the capture antibody. First, 20 µg mL<sup>-1</sup> capture antibody was added to the hybrid device and incubated for 10 min followed by blocking with blocking buffer for another 10 min and washing with PBST. 500 ng mL<sup>-1</sup> CEA was added as a positive control and PBS was added as a negative control. The device was washed with PBST after a 10 min incubation. Different concentrations of polyclonal anti-CEA antibody (1 μg mL<sup>-1</sup>, 5 μg mL<sup>-1</sup>, 10 μg mL<sup>-1</sup>, 15 μg mL<sup>-1</sup>, and 20 µg mL<sup>-1</sup>) were added to both the positive and the negative control for 10 min and washed with PBST. ALPlinked IgG (10 µg mL<sup>-1</sup>) was then added for 7 min and washed three times with PBST. Finally, BCIP/NBT was added for 10 min and the device was disassembled to scan the bottom pond layer with the paper substrate using a portable office scanner or a smartphone camera.

# 2.5 Optimization of the concentration of enzyme-linked secondary antibody

After the optimization of the concentrations of the capture antibody and the anti-CEA polyclonal antibody, the concentration of enzyme-linked secondary antibody (ALP-IgG) was optimized. First, 20  $\mu g$  mL<sup>-1</sup> capture antibody was added to the hybrid device and incubated for 10 min followed by blocking with blocking buffer for another 10 min. The device was washed with PBST followed by the

addition of 500 ng mL $^{-1}$  CEA as a positive control and PBS as a negative control. The device was incubated for 10 min and washed with PBST followed by the addition of 10  $\mu g$  mL $^{-1}$  anti-CEA polyclonal antibody. The device was then incubated for 10 min and washed with PBST. Different concentrations of ALP-linked IgG (1  $\mu g$  mL $^{-1}$ , 3  $\mu g$  mL $^{-1}$ , 6  $\mu g$  mL $^{-1}$ , 9  $\mu g$  mL $^{-1}$ , 12  $\mu g$  mL $^{-1}$ , and 15  $\mu g$  mL $^{-1}$ ) were then added for 7 min and washed three times with PBST. Finally, BCIP/NBT was added for another 10 min and the device was disassembled for image scanning.

#### 2.6 Colorimetric detection of cancer biomarkers

The paper in the PMMA pond hybrid device can be used for the detection of a wide range of biomolecules. Herein, CEA and PSA were detected in the PiPP hybrid device with all the optimized concentrations of different antibodies. For the detection of CEA, 20 μg mL<sup>-1</sup> capture antibody was added to the device and incubated for 10 min followed by blocking with blocking buffer for another 10 min (Fig. 2). Different concentrations of CEA (0.1 ng mL<sup>-1</sup>, 1 ng mL<sup>-1</sup>, 5 ng mL<sup>-1</sup>, 10 ng mL<sup>-1</sup>, 25 ng mL<sup>-1</sup>, 50 ng mL<sup>-1</sup>, and 100 ng mL<sup>-1</sup>) were then added to the device and incubated for 10 min. The device was then washed with PBST followed by the addition of 10 μg mL<sup>-1</sup> anti-CEA polyclonal antibody. 6 μg mL<sup>-1</sup> ALP-linked IgG was then added for 7 min and washed three times with PBST. Finally, BCIP/NBT was added for another 10 min and the device was disassembled for image scanning.

Following a similar procedure for the colorimetric detection of CEA, the detection of PSA was performed by the addition of 20 µg mL<sup>-1</sup> anti-PSA capture antibody and incubation for 10 min. After the substrate was blocked with blocking buffer, different concentrations of PSA (0.1 ng mL<sup>-1</sup>, 1 ng mL<sup>-1</sup>, 5 ng mL<sup>-1</sup>, 10 ng mL<sup>-1</sup>, 25 ng mL<sup>-1</sup>, 50 ng mL<sup>-1</sup>, and 100 ng mL<sup>-1</sup>) were added and incubated for another 10 min. Finally, anti-PSA polyclonal antibody (10 μg mL<sup>-1</sup>) was added followed by the addition of ALP-linked IgG (6 μg mL<sup>-1</sup>) and BCIP/NBT. The devices were scanned using a portable scanner and measured using ImageJ. The signal was calculated as the average of the intensity values of the respective pixels and was subtracted from the maximum value (i.e., 255) to obtain the corrected brightness value which was then used for data analysis. The value obtained with 0 ng mL<sup>-1</sup> biomarker target in PBS was defined as the background. The PiPP device can be reused by changing the paper layer. The device can be sterilized by soaking in 70% ethanol/isopropanol for 15 min and blocked with blocking buffer before reuse.

## 2.7 Cross-reactivity test for CEA and PSA in the hybrid PiPP device

Real-world samples such as blood serum, urine, and cerebrospinal fluid contain various biomolecules with a wide range of concentrations. High specificity is required to screen particular biomarkers, as biomolecules present in the sample may interfere with the detection of target proteins. The

various columns in the PiPP device were used for the specificity test for the detection of CEA. First, 20 µg mL<sup>-1</sup> anti-CEA capture antibody was added to all the columns and incubated for 10 min. The first seven columns from the left were the negative control without the analyte (CEA) and the last column was 25 ng mL<sup>-1</sup> CEA. Following a similar procedure to that of CEA detection, 200 ng mL<sup>-1</sup> IgG, HBsAg, HBcAg, HCVcAg, BSA, and PSA were introduced and analyzed for the specificity test.

Similar to the specificity test for CEA, the specificity test for PSA was performed in the PiPP hybrid device. 20 µg mL<sup>-1</sup> anti-PSA capture antibody was added and incubated for 10 min. The first column from the left was PBS and the second to seventh columns were 200 ng mL<sup>-1</sup> IgG, HBsAg, HBcAg, HCVcAg, BSA, and CEA, respectively, and the last column was  $25 \text{ ng mL}^{-1} \text{ PSA.}$ 

#### 2.8 Multiplexed detection of cancer biomarkers in the PiPP device

A high anti-interference and multiplexed detection capability is required for the wide applicability of the device to screen varieties of disease biomarkers. Here, the device has been used for multiplexed anti-interference detection of CEA and PSA. The first four columns from the left were coated with the anti-CEA capture antibody while the last four columns were coated with the anti-PSA capture antibody. The first and fifth columns were the negative control with PBS. The second and fourth columns were CEA (10 ng mL<sup>-1</sup>), while the sixth and eighth columns were PSA (10 ng mL<sup>-1</sup>). For the antiinterference test of CEA and PSA, both the third and seventh columns consisted of 10 ng mL<sup>-1</sup> CEA, 200 ng mL<sup>-1</sup> HBsAg, 200 ng mL<sup>-1</sup> HCVcAg, and 10 ng mL<sup>-1</sup> PSA. Different combinations of antigens were incubated for 10 min followed by thorough washing and the addition of secondary antibody, following an optimized ELISA procedure.

#### 2.9 Detection of cancer biomarkers in human serum using the PiPP device

To validate the developed hybrid microfluidic microplate and to test its feasibility for real human sample detection, CEA and PSA were spiked in normal human serum. 10 µL of varying concentrations of CEA and PSA were spiked into 1.0 mL human serum which was pre-diluted 3-fold using PBS to obtain the final concentrations of 1 ng mL<sup>-1</sup>, 5 ng mL<sup>-1</sup>, and 10 ng mL<sup>-1</sup>, respectively. After mixing thoroughly, the spiked samples were used for the rapid detection of CEA and PSA by the PiPP hybrid device, and spike recoveries were calculated.

## 3. Results and discussion

### 3.1 Optimization of the concentration of the capture antibody

Optimization of the concentration of the capture antibody was carried out by performing the immunoassay of CEA with

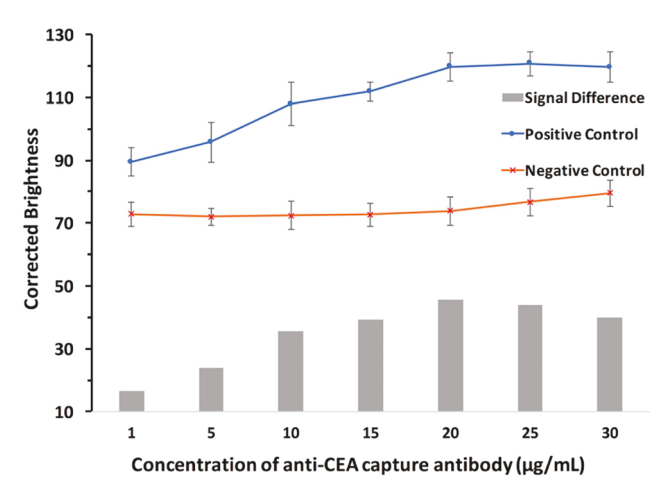


Fig. 3 Optimization of the concentration of anti-CEA capture antibody. The line graph shows the brightness values for the positive (500 ng mL<sup>-1</sup> CEA) and negative (PBS) control with varying concentrations of the anti-CEA capture antibody in the presence of 10 μg mL<sup>-1</sup> anti-CEA polyclonal antibody and 10 μg mL<sup>-1</sup> ALP-linked lgG. The bar graph shows the signal difference between the positive and the negative control (n = 6).

varying concentrations of the anti-CEA capture antibody. As seen from Fig. 3, the brightness value of the positive control (500 ng mL<sup>-1</sup> CEA) increased with the increase in the concentration of the capture antibody from 1 µg mL-1 to 20 μg mL<sup>-1</sup>. It reached a plateau at 20 μg mL<sup>-1</sup> and remained constant with a further increase in the concentration of the capture antibody. For the negative control (PBS) the corrected brightness value remained constant with the increase in the concentration of the capture antibody from 1  $\mu g\ mL^{-1}$  to 20  $\mu g\ mL^{-1}.$  As the concentration of the capture antibody increased further from 20 μg mL<sup>-1</sup>, there was a slight increase in the corrected brightness value (background noise). It could also be

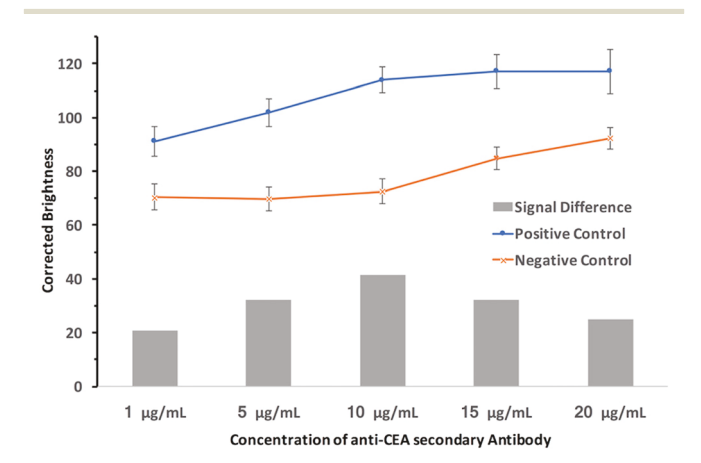


Fig. 4 Optimization of the concentration of polyclonal anti-CEA antibody. The line graph shows the brightness value for the positive (500  $\text{ng} \ \text{mL}^{-1} \ \text{CEA}$ ) and negative (PBS) control with varying concentrations of the anti-CEA polyclonal antibody, in the presence of 20 μg mL<sup>-1</sup> capture antibody and 10 μg mL<sup>-1</sup> ALP-linked IgG. The bar graph shows the signal difference between the positive and the negative control (n = 6).

**Paper** 

observed from Fig. 3 that the signal difference between the positive control and the negative control (*i.e.*, net signal value) was maximum at the capture antibody concentration of 20  $\mu g$  mL<sup>-1</sup>; thereafter it started decreasing because of an increase in the background noise. Therefore, 20  $\mu g$  mL<sup>-1</sup> capture antibody was considered as the optimum concentration for the colorimetric ELISA on the PiPP hybrid devices

# 3.2 Optimization of the concentration of polyclonal anti-CEA secondary antibody

The concentration of the polyclonal anti-CEA antibody was optimized after the optimization of the concentration of the capture antibody. As observed from Fig. 4, the brightness value of the positive control (500 ng mL<sup>-1</sup> CEA) increased with the increase in the concentration of the anti-CEA polyclonal antibody from 1 µg mL-1 to 10 µg mL-1 and it reached a plateau afterward. The average brightness value of the positive control remained almost constant even in the presence of >10 µg mL<sup>-1</sup> polyclonal anti-CEA antibody. For the negative control (PBS) the brightness value remained constant with the increase in the concentration of capture antibody from 1 µg mL<sup>-1</sup> to 10 µg mL<sup>-1</sup>. As the concentration of anti-CEA polyclonal antibody increased further above 10 μg mL<sup>-1</sup>, there was a noticeable increase in the brightness value (background noise). It could also be observed from Fig. 4 that the signal difference between the positive control and the negative control was maximum at the anti-CEA polyclonal antibody concentration of 10 µg mL<sup>-1</sup>, after which there was no increase in signal for the positive control but a sharp increase in background noise. Therefore, 10 µg mL<sup>-1</sup> anti-CEA secondary antibody was considered as an optimum concentration and all the subsequent ELISA assays were performed with 20 µg mL<sup>-1</sup> capture antibody and 10 µg mL-1 the anti-CEA secondary antibody.

# 3.3 Optimization of the concentration of enzyme-linked secondary antibody

The optimal concentration of ALP-linked IgG was optimized after the optimization of the concentrations of the capture antibody and the anti-CEA polyclonal antibody. As seen from Fig. 5, the brightness value of the positive control (500 ng mL<sup>-1</sup> CEA) increased with the increase in the concentration of ALPlinked IgG from 1 µg mL-1 to 6 µg mL-1, after which it reached a plateau and remained almost constant even with any further increase in the concentration of ALP-linked IgG from 6  $\mu g~mL^{-1}$  to 15  $\mu g~mL^{-1}.$  For the negative control (PBS) the brightness values remained constant with the increase in the concentration of ALP-linked IgG from 1 µg mL-1 to 6 μg mL<sup>-1</sup>. As the concentration of ALP-linked IgG increased further from 6 μg mL<sup>-1</sup> to 15 μg mL<sup>-1</sup>, there was a rapid increase in the brightness value (background noise). It could also be seen from Fig. 5 that the signal difference between the positive control and the negative control was maximum

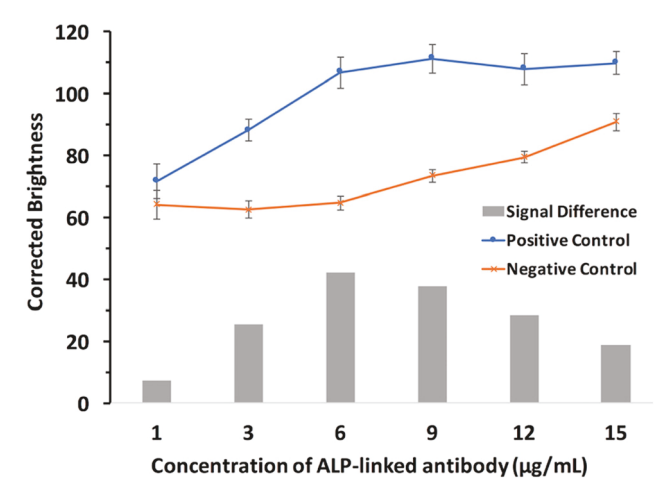


Fig. 5 Optimization of the concentration of the ALP-linked antibody. The line graph shows the brightness values for the positive (500 ng mL $^{-1}$  CEA) and negative (PBS) control with varying concentrations of the ALP-linked antibody in the presence of 20  $\mu$ g mL $^{-1}$  capture antibody and 10  $\mu$ g mL $^{-1}$  anti-CEA polyclonal antibody. The bar graph shows the signal difference between the positive and the negative control (n=6).

at the ALP-linked IgG concentration of 6  $\mu g$  mL<sup>-1</sup>. Therefore, 6  $\mu g$  mL<sup>-1</sup> ALP-linked IgG was considered as the optimum concentration and all the further assays were performed with 20  $\mu g$  mL<sup>-1</sup> capture antibody, 10  $\mu g$  mL<sup>-1</sup> anti-CEA secondary antibody, and 6  $\mu g$  mL<sup>-1</sup> ALP-linked IgG.

# 3.4 Colorimetric detection of cancer biomarkers on the PiPP device

After optimization, rapid ELISA of the cancer biomarkers including CEA and PSA was achieved on the paper-inpolymer-pond hybrid device. Fig. 6A shows the image scanned by a desktop scanner for the quantitative detection of CEA on a PiPP hybrid microfluidic device. It can be observed from Fig. 6A that PBS shows the brightest color and 100 ng mL<sup>-1</sup> CEA shows the darkest purple color, while the purple color of other concentrations darkened from 0.1 ng mL<sup>-1</sup> to 100 ng mL<sup>-1</sup>. After calculating the signal intensity of the scanned images by ImageJ, a calibration curve of the brightness value against the concentration of CEA was plotted as shown in Fig. 6B. The inset in Fig. 6B shows that a linearity range was found over the clinically relevant range from 1 ng mL<sup>-1</sup> to 100 ng mL<sup>-1</sup> with a linear regression of  $y = 27.05 \log(x) + 95.86$  ( $R^2 = 0.98$ ). The LOD of CEA using the hybrid PiPP microfluidic device was found to be 0.32 ng mL<sup>-1</sup> based on the 3-fold SD value above the blank value, which was sensitive enough to detect the clinical cutoff value of 5 ng mL<sup>-1</sup>.<sup>27</sup> Our device was more sensitive as compared to colorimetric immunoassay based upon gold nanoparticles (LOD of 2.32 ng mL<sup>-1</sup>), distance-based assays on paper-based microfluidics (LOD of 2 ng mL<sup>-1</sup>), and microfluidic platforms integrating single bead trapping and acoustic mixing techniques (LOD of 3.1 ng mL<sup>-1</sup>).31,44,45 The sensitivity was even comparable to those of electrochemical

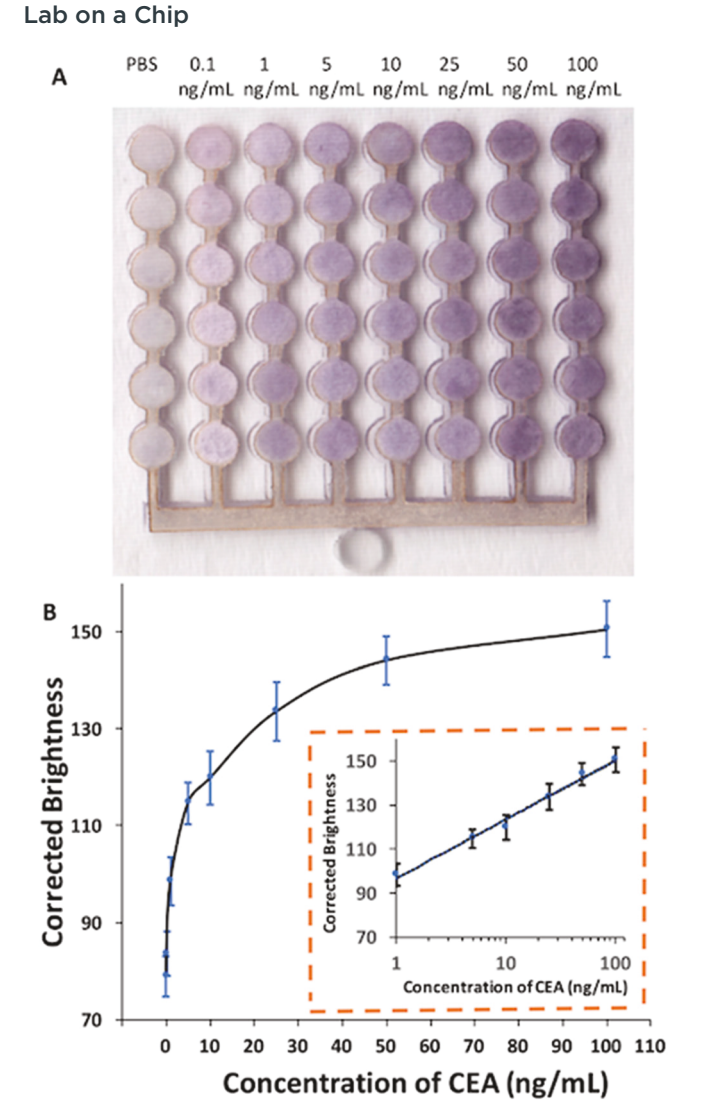


Fig. 6 Rapid quantitative detection of CEA on a PiPP hybrid microfluidic device. (A) Scanned image of the paper substrate by an office scanner after the assay with the negative control (PBS) and different CEA concentrations ranging from 0.1 ng mL<sup>-1</sup> to 100 ng mL<sup>-1</sup>. (B) Calibration curve for the detection of CEA as the brightness value against the concentration of CEA. The inset shows the linear plot of the brightness value of CEA over a logarithmic concentration ranging from 1 ng mL<sup>-1</sup> to 100 ng mL<sup>-1</sup> (n = 6).

detection on microfluidic platforms (LODs of 0.20 ng mL<sup>-1</sup> and 0.3 ng mL<sup>-1</sup>) (Table S1, ESI†). 32,46

Similar to the detection of CEA, rapid colorimetric detection of PSA was also carried out in the PiPP hybrid microfluidic device using the same optimized concentrations of different antibodies. The detection of PSA was performed in the range of 0.1 ng mL<sup>-1</sup> to 100 ng mL<sup>-1</sup>. Fig. 7A shows the image scanned by a desktop scanner for the detection of PSA in a PiPP hybrid microfluidic device. It can be observed that the purple color intensified from PBS to 100 ng mL<sup>-1</sup> PSA. Fig. 7B shows the calibration curve of the brightness of different concentrations of PSA. The inset in Fig. 7B shows that a linearity range was found to cover the clinically relevant range from 0.1 ng mL<sup>-1</sup> to 100 ng mL<sup>-1</sup>

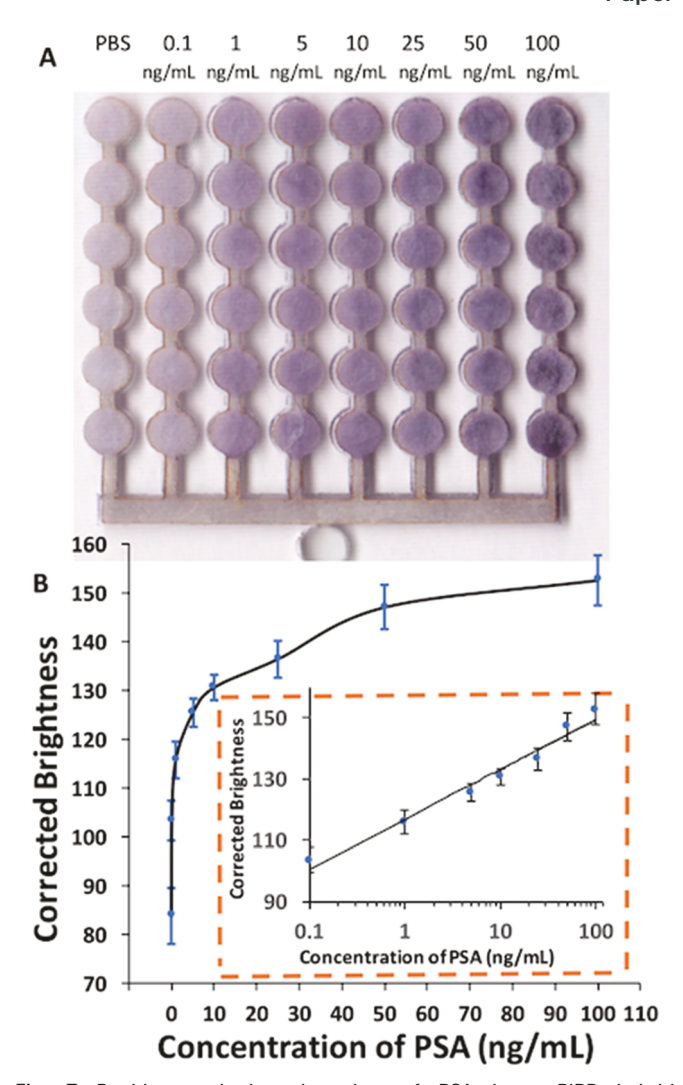


Fig. 7 Rapid quantitative detection of PSA in a PiPP hybrid microfluidic device. (A) A scanned image of the paper substrate by an office scanner after the assay with the negative control (PBS) and different PSA concentrations ranging from  $0.1~\text{ng mL}^{-1}$  to  $100~\text{ng mL}^{-1}$ . (B) Calibration curve for the detection of PSA as brightness against the concentration of PSA. The inset shows the linear plot of the brightness of PSA over a logarithmic concentration range from 1 ng mL<sup>-1</sup> to 100 ng mL $^{-1}$  (n = 6).

with a linear regression of  $y = 16.26 \log(x) + 116.74$  ( $R^2 =$ 0.98). The LOD of PSA using the PiPP hybrid microfluidic device was calculated to be 0.20 ng mL<sup>-1</sup> based on 3-fold SD above the blank value, which is sensitive enough to detect the clinical cutoff value of 4 ng mL<sup>-1</sup>. The sensitivity of the device was better than that of our previous nanoparticlemediated bioassay using a thermometer (LOD of 1.0 ng mL<sup>-1</sup>) and colorimetric assay (LOD of 1.0 ng mL<sup>-1</sup>). <sup>26,47</sup> The LOD of our device was also better than that obtained with PSAconjugated gold nanoparticles based on localized surface plasmon resonance (LOD of 5 ng mL<sup>-1</sup>) and a microfluidicbased multiplexed immunoassay system integrated with an array of QD-encoded microbeads (LOD of 1 ng mL<sup>-1</sup>) (Table S1, ESI†).48,49 Our device was also found to exhibit similar detection sensitivity to the microfluidic electrochemical

detection method which also required a syringe pump (LOD of 0.20 ng mL<sup>-1</sup>).<sup>46</sup>

# 3.5 Cross-reactivity test for CEA and PSA in the PiPP hybrid device

A cross-reactivity test for the detection of CEA and PSA was performed to investigate potential interferences from other biomolecules using some common interfering substances such as IgG, HBsAg, HBcAg, and HCVcAg. As seen from Fig. 8, for the specificity detection of CEA, there was color production only in the last column where 25.0 ng mL $^{-1}$  CEA was added as the analyte. All the other columns (first seven) showed minimum production of color and were significantly different from CEA (p < 0.05), indicating that the test is specific for CEA and other interfering proteins even with very high concentration (200.0 ng mL $^{-1}$ ) do not interfere with the detection of CEA.

Similar to the specificity test for CEA, the specificity test for PSA was performed in the PiPP hybrid device. As

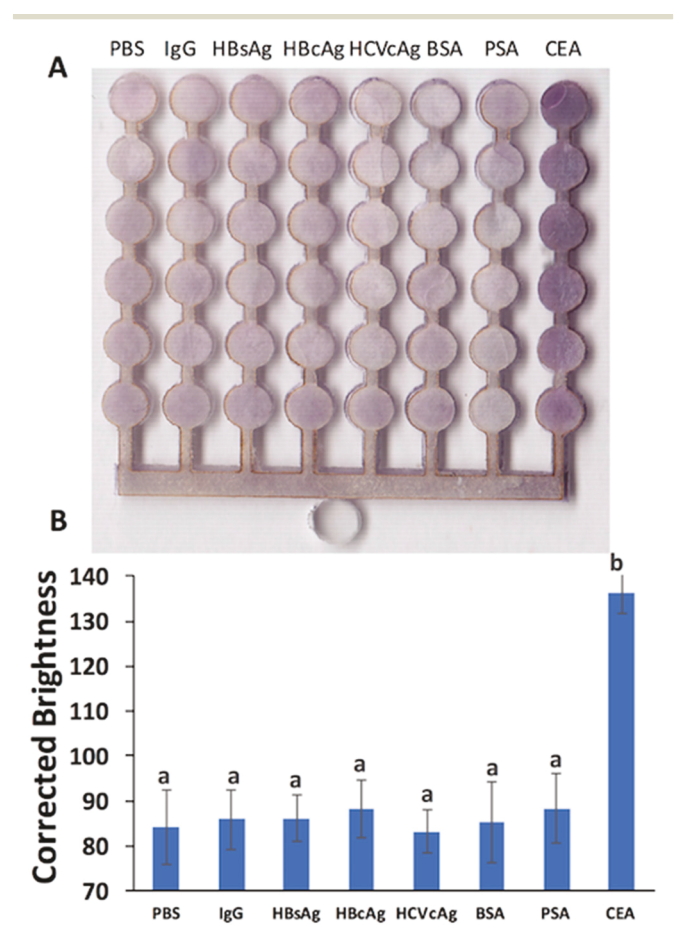


Fig. 8 Specificity test for the detection of CEA in the hybrid PiPP microfluidic device. (A) The scanned image of the chip after the completion of the assay. (B) The brightness of the scanned image of ELISA for specificity detection in the chip. Analytes from left to right: PBS, IgG, HBsAg, HBcAg, HCVcAg, BSA, PSA, and CEA. Different letters on the bar, "a" and "b", show that the data are insignificantly ("a") or significantly different ("b"); p < 0.05; n = 6.

shown in Fig. 9, the first to seventh columns were PBS, 200.0 ng mL<sup>-1</sup> IgG, HBsAg, HBcAg, HCVcAg, BSA, and CEA, respectively, and the last column was 25.0 ng mL<sup>-1</sup> PSA. The detection was specific for PSA, as color production was observed only in the last column. All other interfering proteins did not cross-react with anti-PSA antibody so there was minimum production of color in the first seven columns. These assays show high specificity of our method for the detection of not only CEA but also PSA.

# 3.6 Multiplexed detection of cancer biomarkers in the PiPP device

To demonstrate that the PiPP device has an efficient multiplex biomarker sensing capability, the PiPP device was used for the simultaneous colorimetric detection of multiple cancer biomarkers and negative controls, specifically CEA and PSA (Fig. 10). The second and sixth columns are for the detection of 10 ng mL<sup>-1</sup> CEA and PSA, respectively, and show high purple color density. The third and seventh columns are for the anti-interference test of CEA and PSA, in which

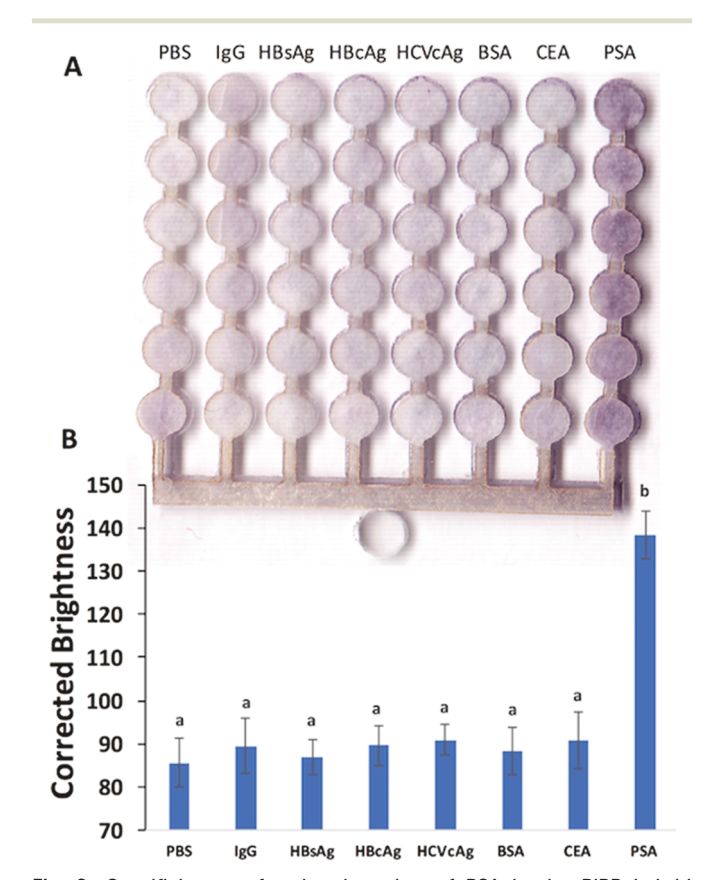


Fig. 9 Specificity test for the detection of PSA in the PiPP hybrid microfluidic device. (A) The scanned image of the chip after the completion of the assay. (B) The brightness of the scanned image of ELISA for specificity detection of PSA in the chip. Analyte from left to right: PBS, IgG, HBsAg, HBcAg, HCVcAg, BSA, CEA, and PSA. Different letters on the bar, "a" and "b", show that the data are insignificantly ("a") or significantly different ("b"); p < 0.05; n = 6.

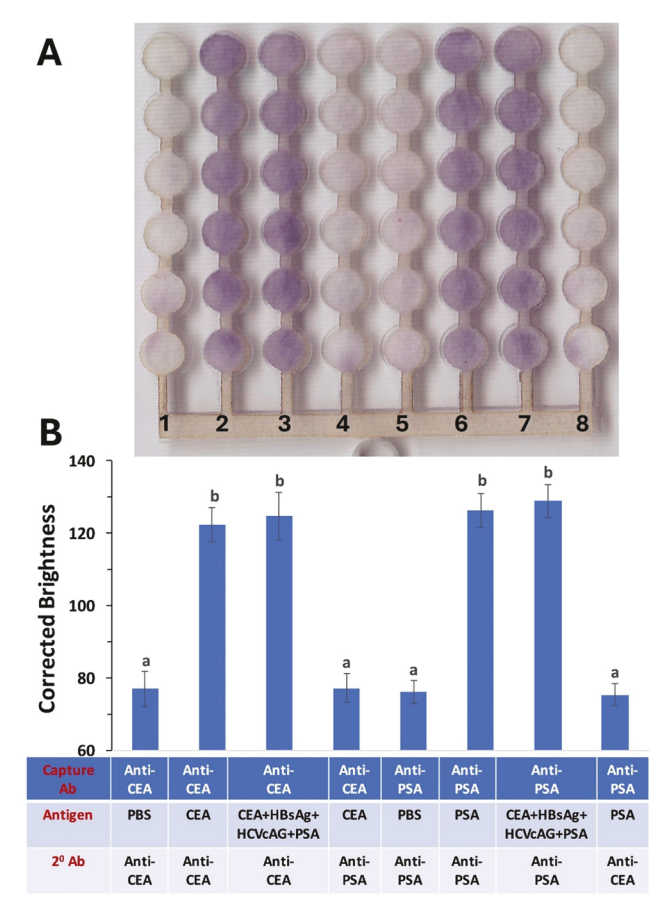


Fig. 10 Multiplexed assay of CEA and PSA in the PiPP hybrid device. (A) Scanned image of the enzyme-catalyzed substrate. (B) Bar plot of the brightness of the scanned image. The bottom section in (B) shows their corresponding capture antibody, antigen, and secondary antibody for each column. Samples: PBS (#1 and #5), CEA (#2 and #4), CEA + HBsAg + HCVcAg + PSA (#3 and #7), and PSA (#5 and #8). Different letters on the bar, "a" and "b", show that the data are insignificantly ("a") or significantly different ("b"); p < 0.05; n = 6.

samples contained a mixture of CEA + HBsAg + HCVcAg + PSA. Even in the presence of a high concentration of interfering proteins like HBsAg and HCVcAg, they produced an equally high density of purple color to samples without interfering agents (*i.e.*, columns #3 and #2 and columns #7 and #6; insignificantly different). The first, fourth, fifth, and eighth columns do not show a purple color as they are either negative controls with PBS (first and fifth) or non-specific secondary antibody (fourth and eighth). This assay showed that our PiPP hybrid device can perform specific simultaneous detection of multiple biomarkers with high anti-interference capability.

# 3.7 Detection of cancer biomarkers in human serum using the PiPP device

To validate the analytical accuracy and to determine its feasibility for the detection of real human samples of cancer biomarkers, normal human serum was spiked with different concentrations of standard CEA and PSA, respectively. Three different concentrations of CEA and PSA (1 ng mL $^{-1}$ , 5 ng mL $^{-1}$ , and 10 ng mL $^{-1}$ ) within the range of linearity and above the LOD were chosen for spiking and recovery tests. As listed in Table 1, most analytical recoveries of the serum samples ranged from 90.0% to 110.4% and were within the acceptable criteria for bio-analytical validation. Percentage recovery = (measured concentration – spiked concentration)/spiked concentration × 100.

## 4. Conclusions

We have developed a simple low-cost paper-in-polymer-pond (PiPP) hybrid microfluidic microplate for the multiplexed quantitative detection of cancer biomarkers with high detection sensitivity. This colorimetric PiPP hybrid microfluidic device takes advantage of both paper and PMMA substrates. The presence of the 3D microporous paper substrate within the pond-shaped structure of the hybrid device ensures that proteins are immobilized within a short period of time without any complicated surface modifications so that the entire assay can be completed within an hour. The PiPP device is also reusable by replacing the paper layer. The flow-through reservoirs aid efficient washing, thus decreasing the background noise and increasing the sensitivity of the ELISA. In addition, the channels in the top PMMA layer can deliver reagents to many microwells (48 microwells herein, but can be scaled up) efficiently and rapidly, enabling higher-throughput analysis without using costly robotic equipment. The results can be observed by the naked eye for qualitative/semiquantitative analysis or scanned by a regular office scanner/smartphone camera for quantitative analysis using ImageJ or smartphone apps.36,51 After the optimization of different conditions, colorimetric ELISA detection of two cancer biomarkers including CEA and PSA using the PiPP hybrid microplate was successfully achieved without using any specialized equipment. LODs of 0.32 ng mL<sup>-1</sup> for CEA and 0.20 ng mL<sup>-1</sup> for PSA were achieved, which were about 10-fold better than that obtained using commercial ELISA kits. Although proof-of-concept testing of the PiPP device was demonstrated using spiked serum samples, the PiPP device's diagnostic effectiveness in real-world clinical settings would still need to be further validated using clinical samples in the future. But given these significant features, this low-cost PiPP hybrid microfluidic

**Table 1** Detection of CEA and PSA spiked in human serum samples by colorimetric ELISA on a hybrid PiPP device

| Sample # | Serum<br>type | Spiked serum concentration (ng mL <sup>-1</sup> ) | Measured values (ng mL <sup>-1</sup> ) | Recovery (%) |
|----------|---------------|---|--|--------------|
| 1        | CEA           | 1   | 1.10                                   | 110.4        |
| 2        | CEA           | 5   | 5.38                                   | 107.6        |
| 3        | CEA           | 10  | 10.58                                  | 105.8        |
| 4        | PSA           | 1   | 0.90                                   | 90.8         |
| 5        | PSA           | 5   | 4.54                                   | 90.8         |
| 6        | PSA           | 10  | 8.87                                   | 88.7         |

device may have wide application for rapid, highly sensitive, and quantitative detection of multiple disease biomarkers including cancers, infectious diseases, and other biomolecules, especially for a low-resource setting.

## Data availability

**Paper** 

The data that support the findings will be available upon request following an embargo from the date of publication to allow for commercialization of research findings.

## **Author contributions**

XL and SST conceived the study. Experiments were performed and validated by SST under the guidance of XL. All authors contributed to data discussion, manuscript preparation, and revision.

## Conflicts of interest

XL and SST have submitted a patent application.

## Acknowledgements

We would like to acknowledge financial support from the Cancer Prevention and Research Institute of Texas (CPRIT; RP210165), NIH/NIAID (R41AI162477), and the U.S. NSF (IIP2122712 and CHE2216473). We are also grateful to the prior financial support to our research from the NIH/NIAID (R21AI107415), the NIH/NIGMS (SC2GM105584), the NIH/NIMHD RCMI Pilot grant (5G12MD007593-22), the NIH BUILDing Scholar Summer Sabbatical Award, the NSF (IIP1953841, IIP2052347, and DMR1827745), the DOT (CARTEEH), the Philadelphia Foundation, the Medical Center of the Americas Foundation (MCA), the University of Texas (UT) System for the STARS award, and the UTEP for IDR, URI, and MRAP awards.

#### References

- 1 L. Wang, B. Lu, M. He, Y. Wang, Z. Wang and L. Du, *Front. Public Health*, 2022, **10**, 811044.
- 2 F. Bray, J. Ferlay, I. Soerjomataram, R. L. Siegel, L. A. Torre and A. Jemal, *Ca-Cancer J. Clin.*, 2018, **68**, 394–424.
- 3 J. Ferlay, I. Soerjomataram, R. Dikshit, S. Eser, C. Mathers, M. Rebelo, D. M. Parkin, D. Forman and F. Bray, *Int. J. Cancer*, 2015, **136**, E359–E386.
- 4 H. Grönberg, Lancet, 2003, 361, 859-864.
- 5 J. Ferlay, I. Soerjomataram, R. Dikshit, S. Eser, C. Mathers, M. Rebelo, D. M. Parkin, D. Forman and F. Bray, *Int. J. Cancer*, 2015, 136, E359–E386.
- 6 B. Lu, N. Li, C.-Y. Luo, J. Cai, M. Lu, Y.-H. Zhang, H.-D. Chen, M. Dai and J. Ni, *Chin. Med. J.*, 2021, 134, 1941–1951.
- 7 K. Unger-Saldaña, World J. Clin. Oncol., 2014, 5, 465.
- 8 H. Sung, J. Ferlay, R. L. Siegel, M. Laversanne, I. Soerjomataram, A. Jemal and F. Bray, *Ca-Cancer J. Clin.*, 2021, 71, 209–249.

- 9 G. P. Guy Jr, D. U. Ekwueme, K. R. Yabroff, E. C. Dowling, C. Li, J. L. Rodriguez, J. S. de Moor and K. S. Virgo, J. Clin. Oncol., 2013, 31, 3749.
- 10 D. E. Bloom, E. Cafiero, E. Jané-Llopis, S. Abrahams-Gessel, L. R. Bloom, S. Fathima, A. B. Feigl, T. Gaziano, A. Hamandi and M. Mowafi, *The global economic burden of noncommunicable* diseases, Program on the Global Demography of Aging, 2012.
- 11 M. Arnold, M. S. Sierra, M. Laversanne, I. Soerjomataram, A. Jemal and F. Bray, *Gut*, 2016, **66**(4), 683–691.
- 12 N. P. Sardesai, K. Kadimisetty, R. Faria and J. F. Rusling, *Anal. Bioanal. Chem.*, 2013, 405, 3831–3838.
- 13 O. Pomakov, A Genetic Link Between Prostate Cancer and Colon Cancer, https://drcatalona.com/quest/a-genetic-link-betweenprostate-cancer-and-colon-cancer/, (accessed May 7, 2024).
- 14 G. Fu, S. T. Sanjay, W. Zhou, R. A. Brekken, R. A. Kirken and X. Li, *Anal. Chem.*, 2018, **90**, 5930–5937.
- 15 S. T. Sanjay, G. Fu, M. Dou, F. Xu, R. Liu, H. Qi and X. Li, *Analyst*, 2015, **140**, 7062–7081.
- 16 M. Dou, S. T. Sanjay, M. Benhabib, F. Xu and X. Li, *Talanta*, 2015, 145, 43–54.
- 17 S. T. Sanjay, W. Zhou, M. Dou, H. Tavakoli, L. Ma, F. Xu and X. Li, *Adv. Drug Delivery Rev.*, 2018, 128, 3–28.
- 18 X. J. Li and Y. Zhou, Microfluidic devices for biomedical applications, Elsevier, 2013.
- 19 G. S. Fiorini and D. T. Chiu, *BioTechniques*, 2005, 38, 429-446.
- 20 M. Dou, S. T. Sanjay, D. C. Dominguez, P. Liu, F. Xu and X. Li, *Biosens. Bioelectron.*, 2017, 87, 865–873.
- 21 S. T. Sanjay, M. Dou, G. Fu, F. Xu and X. Li, *Curr. Pharm. Biotechnol.*, 2016, 17, 772–787.
- 22 J. Zhang, H. Tavakoli, L. Ma, X. Li, L. Han and X. Li, Adv. Drug Delivery Rev., 2022, 187, 114365.
- 23 S. S. Timilsina, P. Jolly, N. Durr, M. Yafia and D. E. Ingber, *Acc. Chem. Res.*, 2021, 54, 3529–3539.
- 24 C. Li, W. Zhou, A. G. Ruiz, Y. Mohammadi, Q. Li, S. Zhang, X. Li and G. Fu, *TrAC*, *Trends Anal. Chem.*, 2024, 177, 117809
- 25 S. T. Sanjay, M. Dou, J. Sun and X. Li, Sci. Rep., 2016, 6, 30474.
- 26 G. Fu, S. T. Sanjay, M. Dou and X. Li, Nanoscale, 2016, 8, 5422–5427.
- 27 E. Tan, N. Gouvas, R. J. Nicholls, P. Ziprin, E. Xynos and P. P. Tekkis, *Surg. Oncol.*, 2009, **18**, 15–24.
- 28 M. Zhou, M. Yang and F. Zhou, *Biosens. Bioelectron.*, 2014, 55, 39-43.
- 29 Q. Zhou, Y. Lin, K. Zhang, M. Li and D. Tang, *Biosens. Bioelectron.*, 2018, **101**, 146–152.
- 30 A. I. Barbosa, J. H. Wichers, A. van Amerongen and N. M. Reis, *Bionanoscience*, 2017, 7, 718–726.
- 31 H. Chen, C. Chen, S. Bai, Y. Gao, G. Metcalfe, W. Cheng and Y. Zhu, *Nanoscale*, 2018, **10**, 20196–20206.
- 32 B. Li, L. Yu, J. Qi, L. Fu, P. Zhang and L. Chen, *Anal. Chem.*, 2017, **89**, 5707–5712.
- 33 Z. Qiu, J. Shu and D. Tang, Anal. Chem., 2017, 89, 5152-5160.
- 34 G. Fu, R. Hou, X. Mou and X. Li, *Anal. Chem.*, 2021, 93, 15105–15114.

- 35 A. I. Barbosa, P. Gehlot, K. Sidapra, A. D. Edwards and N. M. Reis, Biosens. Bioelectron., 2015, 70, 5-14.
- 36 S. T. Sanjay, M. Li, W. Zhou, X. Li and X. Li, Microsyst. Nanoeng., 2020, 6, 28.
- 37 K. S. Prasad, X. Cao, N. Gao, Q. Jin, S. T. Sanjay, G. Henao-Pabon and X. Li, Sens. Actuators, B, 2019, 127516.
- 38 D. I. Walsh III, D. S. Kong, S. K. Murthy and P. A. Carr, Trends Biotechnol., 2017, 35, 383-392.
- 39 U. Ali, K. J. B. A. Karim and N. A. Buang, Polym. Rev., 2015, **55**, 678–705.
- 40 J. Zhou, D. A. Khodakov, A. V. Ellis and N. H. Voelcker, Electrophoresis, 2012, 33, 89-104.
- 41 M. Dou, D. C. Dominguez, X. Li, J. Sanchez and G. Scott, Anal. Chem., 2014, 86, 7978-7986.
- 42 P. Zuo, X. Li, D. C. Dominguez and B.-C. Ye, Lab Chip, 2013, 13, 3921-3928.
- 43 H. Tavakoli, E. Hirth, M. Luo, S. Sharma Timilsina, M. Dou, D. C. Dominguez and X. Li, Lab Chip, 2022, 22, 4693-4704.

- 44 X. Jia, T. Song, Y. Liu, L. Meng and X. Mao, Anal. Chim. Acta, 2017, 969, 57-62.
- 45 Y. Chen, W. Chu, W. Liu and X. Guo, Sens. Actuators, B, 2018, 260, 452-459.
- 46 A. Fragoso, D. Latta, N. Laboria, F. von Germar, T. E. Hansen-Hagge, W. Kemmner, C. Gärtner, R. Klemm, K. S. Drese and C. K. O'Sullivan, Lab Chip, 2011, 11, 625-631.
- 47 G. Fu, S. T. Sanjay and X. Li, Analyst, 2016, 141, 3883-3889.
- 48 M. Jazayeri, H. Amani, A. Pourfatollah, A. Avan, G. Ferns and H. Pazoki-Toroudi, Cancer Gene Ther., 2016, 23, 365.
- 49 S. W. Han, E. Jang and W.-G. Koh, Sens. Actuators, B, 2015, 209, 242-251.
- 50 P. van Amsterdam, A. Companjen, M. Brudny-Kloeppel, M. Golob, S. Luedtke and P. Timmerman, Bioanalysis, 2013, 5, 645-659.
- 51 X. Xu, X. Wang, J. Hu, Y. Gong, L. Wang, W. Zhou, X. Li and F. Xu, Electrophoresis, 2019, 40, 914-921.